HiSST: 3rd International Conference on
High-Speed Vehicle Science Technology
14 -19 April 2024, Busan, Korea

Numerical Simulation of Flow/Heat Transfer/Thermal Decomposition Characteristics of Supercritical Hydrocarbon Aviation Fuel in a Mini-channel

Minseo Lee[1], *Hyung Ju Lee*[1]

Abstract

In a cooling channel of a regenerative cooling system of hypersonic cruise vehicles, a hydrocarbon aviation fuel is heated to a supercritical state, which leads to complex interactions between fluid flow, heat transfer, and thermal decomposition reactions. In order to understand such a complicated phenomenon, numerical analyses are conducted investigating the fluid flow resistance, heat transfer characteristics, and endothermic decomposition reactions of hydrocarbon fuel under supercritical conditions. The results showed the pressure drop increase and the Heat Transfer Deterioration (HTD) due to the abrupt variation in thermophysical properties above the pseudo-critical temperature. In addition, the numerical results of the endothermic decomposition reaction using n-dodecane's Proportional Product Distribution (PPD) model confirmed that hydrogen and various light hydrocarbons appeared in good agreement with the existing experimental data.

Keywords: *Hypersonic vehicle, Regenerative cooling system, Endothermic decomposition reaction, Hydrocarbon aviation fuel*

1. Introduction

Hypersonic cruise vehicles can fly over Mach 5 or higher in the atmosphere, and thus they can be used as hypersonic missiles or hypersonic airliners [1,2]. When it comes to developing practical hypersonic cruise vehicles, however, a variety of complex phenomena occur, including aerothermodynamic heating and supersonic combustion, which must be addressed effectively [3]. Fortunately, hydrocarbon aviation fuels absorb a significant amount of heat via thermal cracking or pyrolysis into light hydrocarbons when heated to high temperatures [4-6], and with the application of suitable catalysts, they can undergo catalytic cracking, inducing endothermic reactions even at lower temperatures compared to thermal cracking [7-9]. As a result, they can be circulated as a coolant in an active regenerative cooling system of hypersonic vehicles in order to address the severe heating issues of the airframe and the scramjet engine associated with hypersonic flight. When the heated and decomposed fuel after being circulated in the cooling channel is supplied to the scramjet combustor, furthermore, the efficiency of supersonic combustion can be improved significantly compared to when the fuel is supplied in liquid state, which leads to increase the overall cycle performance of the entire propulsion system [10-13].

When hydrocarbon fuel is heated to above its critical point and pyrolyzed into multiple components in a regenerative cooling system, its thermophysical properties change drastically, which subsequently influences the overall flow and heat transfer characteristics inside the cooling channels. Furthermore, the injection and atomization characteristics of the supercritical and/or cracked fuel become different from those of the original liquid fuel, and this greatly affects its mixing, ignition, and combustion performance in the supersonic combustor [14-16]. As a result, it is essential to establish analytical techniques capable of simulating the complex interactions between fluid flow, heat transfer, and endothermic reactions within mini-channels for the development of an efficient active regenerative

[1] *Pukyong National University, Busan, Republic of Korea, hj.lee@pknu.ac.kr*

cooling system. In this study, therefore, numerical analyses of flow, heat transfer, and endothermic decomposition reactions within a single channel have been conducted and then compared with existing experimental and numerical data obtained from several previous studies in order to facilitate the development of such analytical techniques.

2. Flow Resistance & Heat Transfer Characteristics

2.1. Numerical method

A three-dimensional cylindrical pipe with an inner diameter of 1.8 mm and wall thickness of 0.2 mm was adopted for the channel geometry as shown in Fig. 1. The total numbers of grid cells were 370,000 for the flow resistance estimation in the horizontal configuration and 470,000 for validation and the heat transfer simulation in the vertical downward flow condition. The solver for the current study is the pressure-based, steady RANS (Reynolds-Averaged Navier-Stokes) in ANSYS Fluent 2022 R1, and the k-ω SST turbulence model was applied. In addition, the working fluid for the current preliminary simulations as well as the validation was RP-3 surrogate, of which detail composition is introduced in Ref. [17]. Its thermophysical properties including the density, specific heat, viscosity, and thermal conductivity at a range of the temperature and pressure conditions are obtained from the NIST SUPERTRAPP S/W, and then represented as polynomial fittings for the simulation.

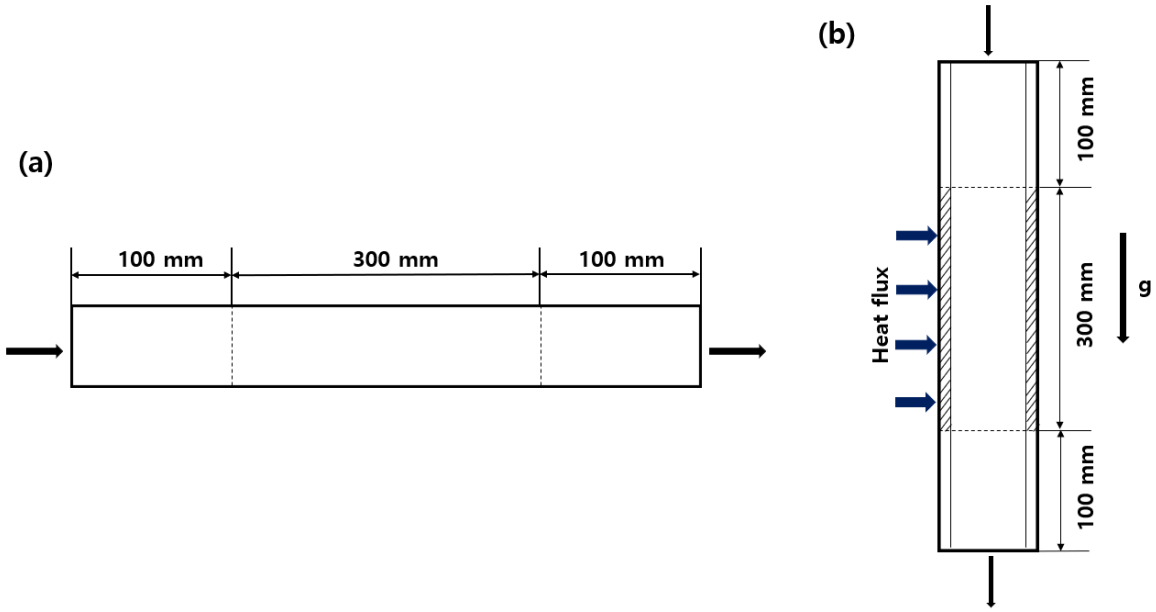

Fig 1. Schematic of physical model for (a) flow resistance estimation and (b) validation and heat transfer analysis

2.2. Validation

In order to verify the simulation models used in this study, a validation was conducted using the geometry depicted in Fig. 1(b), and then compared with existing experimental data as well as Zhu et al.'s computational results [17]. Figure 2 presents the current calculation of the outer wall temperature of the vertical (downward) flow configuration. The inlet temperature, operating pressure, and mass flow rate were set as 473 K, 5 MPa, and 3 g/s, respectively, and the heat flux was varied as 300, 400, 500, and 550 kW/m^2. The variation of the wall temperature along the flow direction confirms that the present simulation can reproduce the experimental data much better than Zhu et al.'s results, with the maximum relative error of only 0.52% in the prescribed operating conditions.

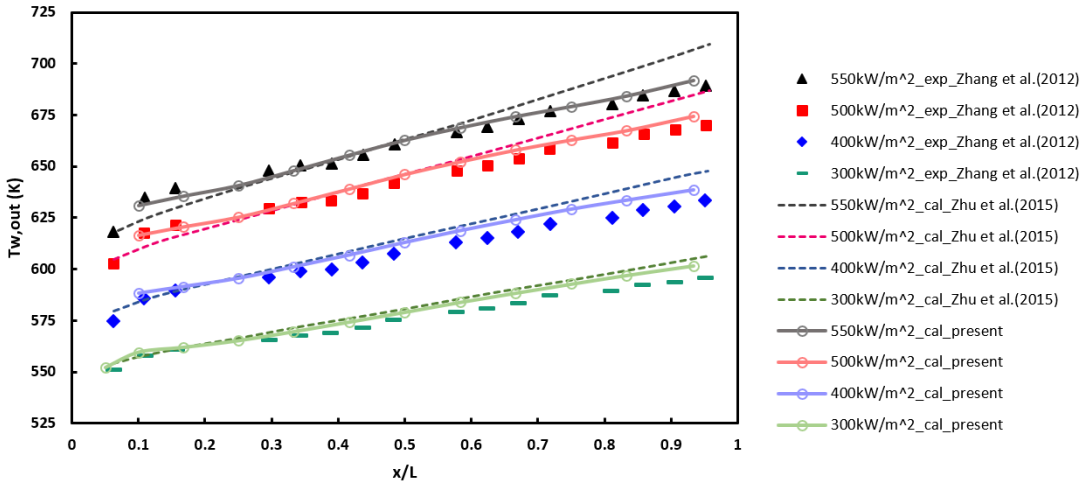

Fig 2. Comparison of the outer wall temperature obtained from the current calculation with existing experiment data as well as Zhu et al.'s simulation [17]

2.3. Flow resistance characteristics

Numerical simulations were conducted on the flow resistance characteristics by calculating the pressure difference between the inlet and outlet of the horizontal flow configuration shown in Fig. 1(a), with the inlet temperatures ranging from 400 K to 750 K, the operating pressures of 3, 4, and 5 MPa, and the constant inlet mass flow rate of 4 g/s. Figure 3 presents the pressure drop with respect to the inlet temperature variation under the given pressure conditions.

When the channel's inlet fluid temperature is lower than the fuel's critical temperature of 640.2 K, the pressure drop slightly decreases or remains almost constant as the temperature increases. However, when the temperature exceeds the critical temperature, the pressure drop increases sharply with temperature elevation. This increasing trend is more pronounced at lower pressures. The reason for this trend is that the density decreases significantly above the critical temperature, leading to an increase in velocity, and the rate of density decrease is more substantial as pressure decreases. The current calculation not only captures the flow resistance characteristics dependent on the pressure and temperature but also align well with the results from the previous computational study by Zhu et al. [17].

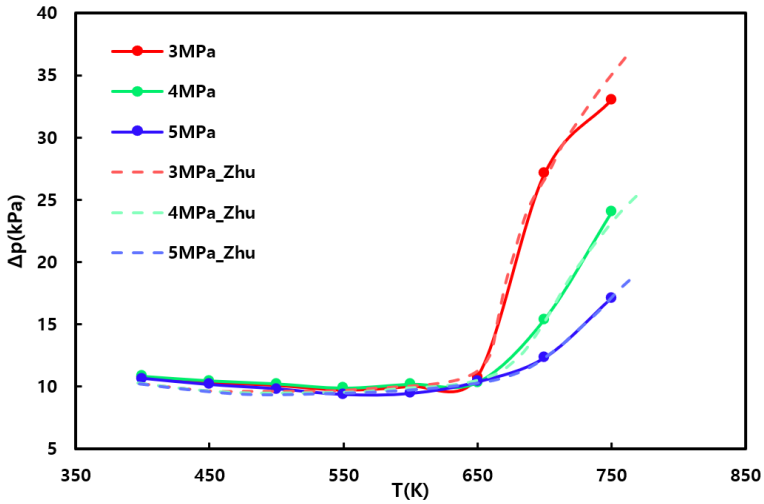

Fig 3. Distribution of the calculated pressure drop with respect to fuel inlet temperature under different operating pressures

2.4. Heat transfer characteristics

Heat transfer characteristics of a supercritical hydrocarbon fuel was also investigated in this section. The inlet fluid temperature and the outlet pressure were set as 373 K and 3 MPa, respectively, and the mass flow rate was varied at 2, 3, 4, and 5 g/s. The heat flux of 300 kW/m^2 and 500 kW/m^2 was applied at the 300 mm section of the wall shown in Fig. 1(b) while the remaining walls were set as adiabatic.

First, the calculated average fluid temperature, wall temperature, and Nusselt number distributions along the tube axis at the heat flux of 300 kW/m^2 are presented in Fig. 4. It is observed clearly from Fig. 4 (a) and (b) that both of the wall temperature and the average flow temperature are increasing continuously along the flow direction. Overall, the predicted temperatures in this study generally show similar trends to Zhu et al.'s results [17], but the predicted temperatures in this study are lower at lower mass flow rates. Based on the validation outcomes, it is deduced that the results of this study are expected to better match experimental values. Additionally, the Nusselt number follows a slight decrease at the inlet and then increases linearly, consistent with the trends observed in Zhu et al. results.

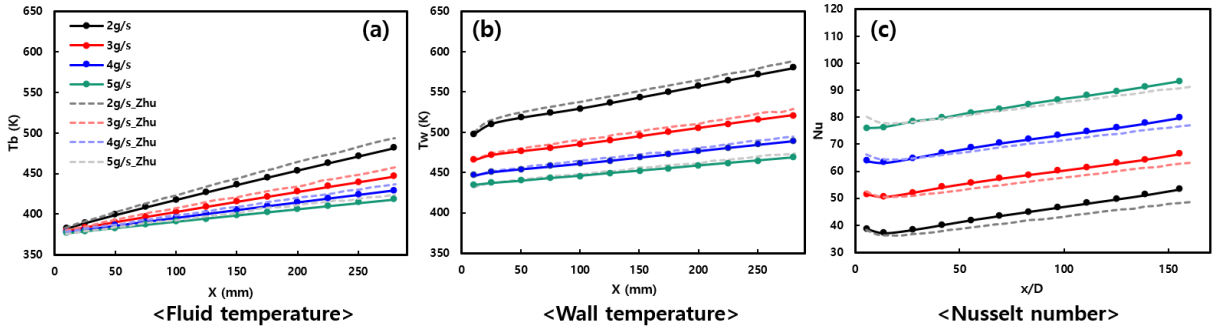

Fig 4. Distributions of (a) the average fluid temperature, (b) the wall temperature, and (c) the Nusselt number, at the heat flux of 300 kW/m^2

Next, the calculated results of the average fluid temperature, wall temperature, and Nusselt number at the heat flux of 500 kW/m^2 are presented in Fig. 5. Similar to the results at 300 kW/m^2, both fluid and wall temperatures show a gradual increase along the channel length. However, as shown in Fig. 5(b), a sudden increase in wall temperature occurs around 180 mm for the case of mass flow rate at 2 g/s. The temperature at this abrupt increase point (approximately at the location of 180 mm) is about 685 K, which corresponds to the pseudo-critical temperature of the RP-3 surrogate. When the wall temperature exceeded the pseudo-critical temperature of 685 K, Heat Transfer Deterioration (HTD) is occurred for the lowest mass flow rate condition due to the sharp variation of thermophysical properties. As a result, the wall temperature increases significantly, causing a decrease in heat transfer coefficients represented by the Nusselt number.

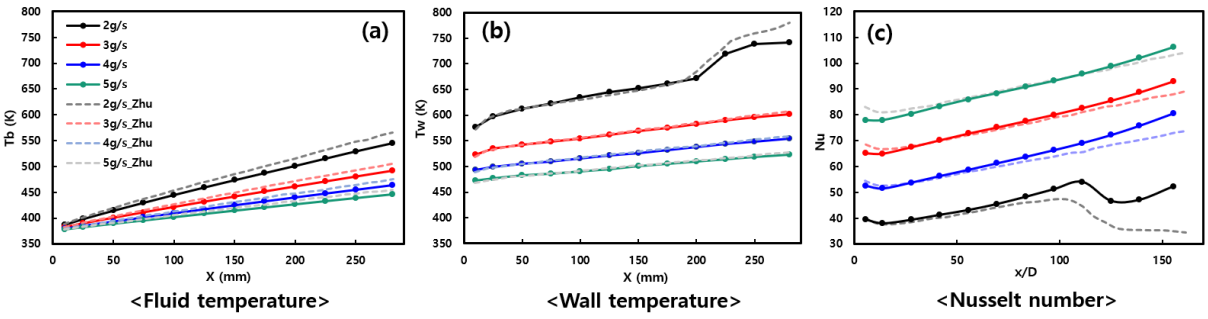

Fig 5. Distributions of (a) the average fluid temperature, (b) the wall temperature, and (c) the Nusselt number, at the heat flux 500 kW/m^2

3. Thermal Decomposition Characteristics

3.1. Analysis domain and mesh system

For the numerical analysis of thermal decomposition, a 2-D axisymmetric horizontal cylindrical duct was employed representing the typical mini-channel configuration considered in a previous study [19]. The total length of the duct was set to 1,100 mm, with the length of 950 mm from the inlet designated as the heating section and the remaining length of 150 mm as adiabatic. A structured grid system was utilized, and fine grids were generated near the wall so that the y+ value was maintained below 5 in order to simulate accurately the interactions between the wall and the fluid. A total of 220,000 grids were generated, and the entire configuration and the resultant grid system are illustrated in Fig. 6.

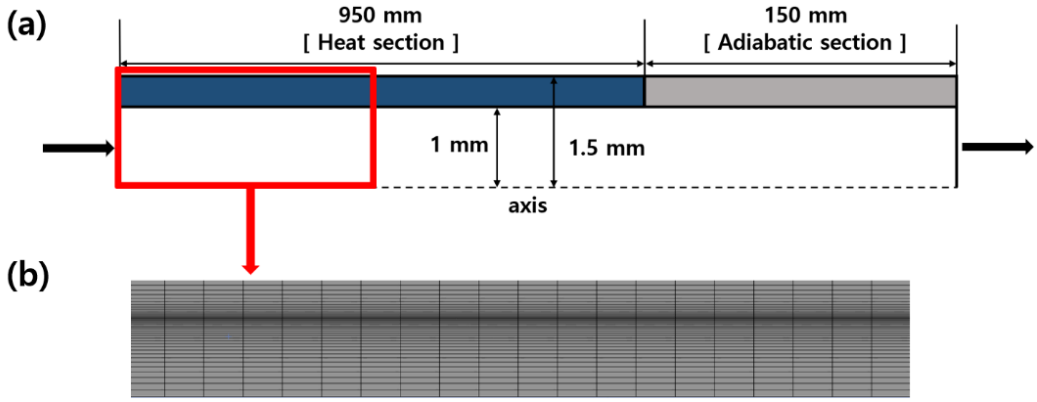

Fig 6. Schematic of (a) the cylindrical tube and (b) the mesh system

3.2. Analysis model

The numerical simulation was conducted using ANSYS Fluent 2022 R1. A 2D steady RANS was adopted, and the k-ω SST model was employed for turbulence modeling. In order to calculate the thermal decomposition chemical reaction, the Finite-Rate/Eddy-Dissipation model was applied as the Reaction model. Detailed analysis models are presented in Table 1. Based on the composition of chemical reaction products, the density and specific heat of the working fluid are calculated by the volume-weighted mixing-law and mixing-law, respectively, whereas both the thermal conductivity and the viscosity are calculated by the mass weighted-mixing-law.

Table 1. Numerical settings

Parameter	Value
Solver	2D, pressure-based, steady RANS
Pressure-velocity coupling	SIMPLEC
Flux type	Rhie-Chow: distance based
Spatial discretization, gradient	Least squares cell based
Spatial discretization, flow and others	Second order upwind
Turbulence model	k-ω SST
Reaction model	Species Transport: Volumetric Finite-Rate/Eddy-Dissipation

3.3. Boundary conditions

In this study, n-dodecane ($C_{12}H_{26}$) was utilized as the working fluid to analyze the endothermic decomposition reaction of hydrocarbon aviation fuel. In order to simulate the supercritical state inside the mini-channel, the boundary conditions were set higher than the critical pressure (1.806 MPa) and temperature (658.1 K) of n-dodecane. The mass flow rate at the inlet was fixed as 3 kg/h. The heat flux was set to represent the conversion rate of n-dodecane in the decomposition reaction model. Therefore, the heat flux of 65 kW/m^2 was uniformly applied within the solid walls for the primary cracking analysis while the heat flux of 160 kW/m^2 was applied for the analysis of including the secondary cracking. The calculation conditions are presented in Table 2. Additionally, all the properties of n-dodecane and the generated chemical species were obtained from the NIST SUPERTRAPP. These properties were represented by piecewise-polynomial fits for the temperature range from 300 K to 1000 K to be implemented in the simulation.

Table 2. Simulation conditions

Parameter	Value
Working fluid	n-dodecane
Pressure	3 MPa
Inlet temperature	665 K
Mass flow rate	3 kg/h
Heat flux	65 kW/m^2 (primary cracking) 160 kW/m^2 (secondary cracking)

3.4. Chemical reaction mechanism

For the numerical analysis of thermal decomposition reaction inside the mini-channel, a chemical reaction mechanism considering the concerning parameters such as pressure and temperature of the fuel's pyrolysis is required. In this study, the proportional product distribution (PPD) model for n-dodecane, a global one-step reaction model developed by Zhang et al. [20], was adopted.

The thermal decomposition of n-dodecane can be divided into three regions: primary, secondary, and severe. Firstly, it is stated in Ref. [20] that when the temperature of the fuel is below 530°C, the fuel conversion rate increases slowly. This region is referred to as primary cracking. In the primary cracking region, the fuel conversion rate corresponds up to 13%, and the associated one-step global reaction is represented by Eq. (1) as follows.

$$\begin{aligned} C_{12}H_{26} \rightarrow\ & 0.0314H_2 + 0.2368CH_4 + 0.3940C_2H_4 + 0.3595C_2H_6 \\ & +0.2855C_3H_6 + 0.2294C_3H_8 + 0.0816C_4H_8 + 0.0430C_4H_{10} \\ & +0.1560C_8H_{18} + 0.8496C_8H_{16} + 0.0187C_9H_{12} \end{aligned} \quad (1)$$

Here, the reaction rate constant is expressed by the Arrhenius equation, given by Eq. (2); A is the pre-exponential factor and set as 2.466 x 10^{14}, and E_a is the activation energy and set as 225.8 kJ/mol.

$$\ln k = \ln A - \frac{E_a}{RT} \quad (2)$$

Next, the secondary cracking is reported to occur between 530°C and 600°C, where the fuel conversion rate rapidly increases up to 70.9% [20]. In this secondary cracking phase, the PPD model considers the decomposition of chain alkanes and alkenes with increasing fuel conversion rate, leading to the

generation of additional species, including monocyclic aromatic hydrocarbons (MAHs). This is represented by the following equations (3) and (4). Here, C_8H_{18} represents chain alkanes while C_8H_{16} represents chain alkenes.

$$\begin{aligned} C_8H_{18} \rightarrow\ & 0.0584H_2 + 0.5303CH_4 + 0.7551C_2H_4 \\ & +0.5460C_2H_6 + 0.5518C_3H_6 + 0.2862C_3H_8 \\ & +0.1551C_4H_8 + 0.0672C_4H_{10} + 0.1627C_9H_{12} \end{aligned} \tag{3}$$

$$\begin{aligned} C_8H_{16} \rightarrow\ & 0.0453H_2 + 0.4128CH_4 + 0.6219C_2H_4 \\ & +0.4288C_2H_6 + 0.4328C_3H_6 + 0.2262C_3H_8 \\ & +0.1456C_4H_8 + 0.0531C_4H_{10} + 0.2042C_9H_{12} \\ & +0.0611C_7H_8 + 0.0641C_7H_{12} \end{aligned} \tag{4}$$

Similarly, the reaction rate constant is expressed by the Arrhenius equation, given by Eq. (2); the pre-exponential factor is 7.385×10^{14} and 2.631×10^{14} for chain alkanes and chain alkenes, respectively, and the activation energies are 209.6 kJ/mol and 217.8 kJ/mol for chain alkanes and chain alkenes, respectively.

3.5. Primary thermal cracking results

To assess the effect of primary cracking, where the fuel conversion rate reaches 13%, comparisons were made between the fluid temperature and the mass fraction of n-dodecane within the mini-channel. As depicted in Fig. 7(a), in the simulation without the PPD model (i.e., without the thermal decomposition reaction), the maximum fluid temperature reaches 850 K, whereas when the PPD model is applied, the maximum temperature is reduced to 830 K due to the endothermic thermal decomposition reaction of n-dodecane. Additionally, Fig. 7(b) illustrates the mass fraction of the fuel along the channel length. It is evident that a sharp decrease in mass fraction begins around 0.5 m, and comparing the results of the temperature profile, the temperature difference between the two cases of with and without the thermal decomposition is observed to increase around 0.5 m, indicating that the simulation effectively captures the endothermic reaction.

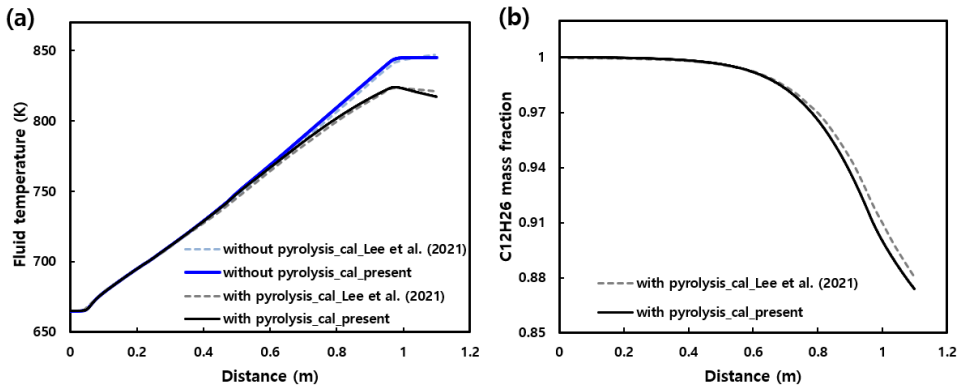

Fig 7. (a) Fluid temperature at the axis and (b) Mass fraction of n-dodecane for the primary cracking simulation

Fig. 8 presents the comparison of the mass fractions of gaseous chemical species generated from the thermal decomposition reactions between the numerical analysis and the experimental data [20], along with previous numerical results [19]. All of the eight chemical species show a linear increase in mass

fraction with increasing conversion rate of n-dodecane, closely matching the experimental results. Therefore, it can be concluded that the analysis effectively simulates the phenomenon of hydrocarbon fuel decomposing into hydrogen and various low molecular-weight hydrocarbons.

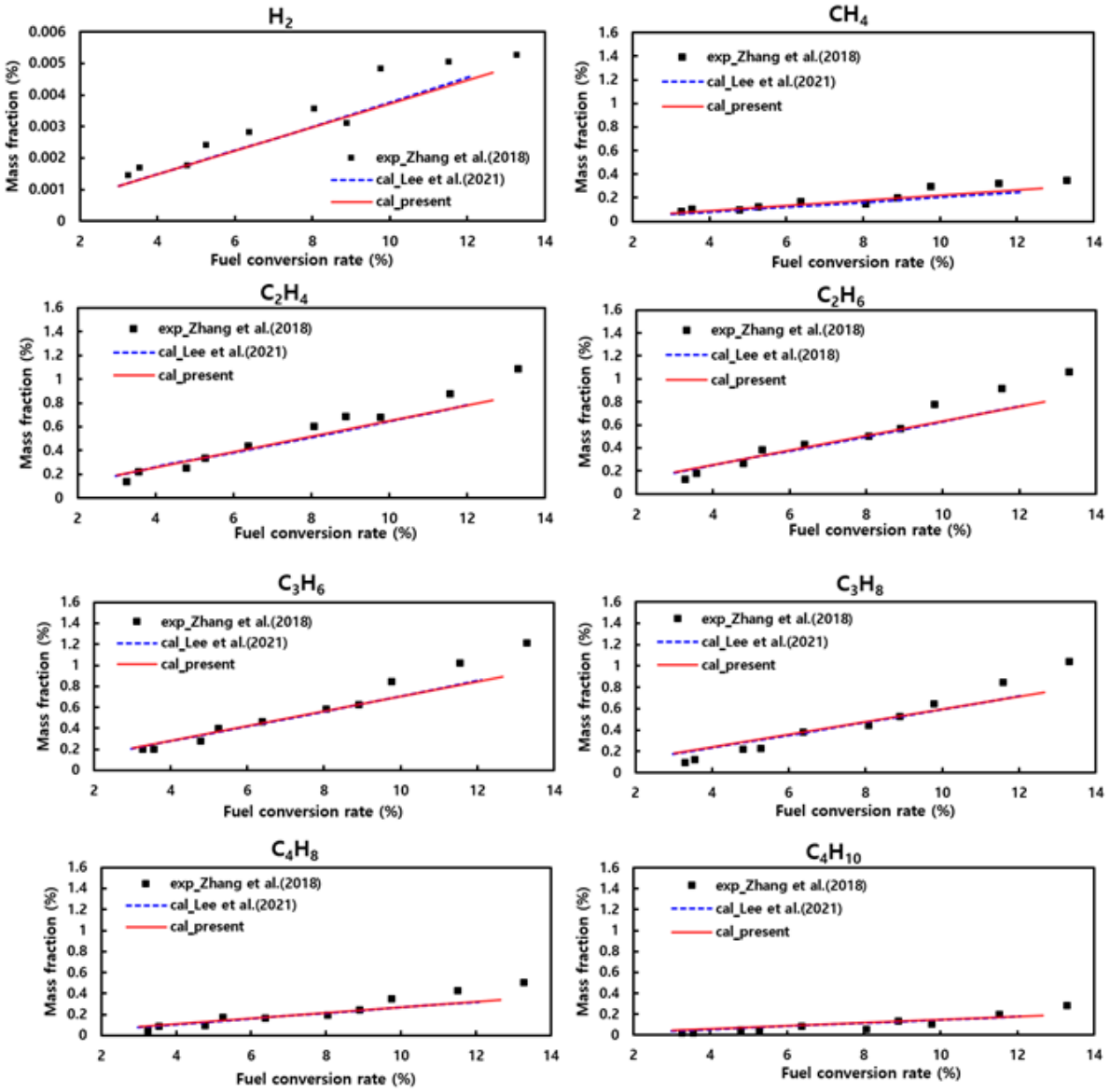

Fig 8. Mass fraction of products species from experiments and numerical simulation for the primary cracking

3.6. Secondary thermal cracking results

The secondary cracking which occurs when the fuel conversion rate exceeds 13% involves additional decomposition of chain alkanes and alkenes represented by C_8H_{18} and C_8H_{16}, respectively. As a result, monocyclic aromatic hydrocarbons (MAH) and cycloalkenes are produced, represented by C_7H_8 (toluene) and C_7H_{12} in the PPD model, respectively.

Fig. 9 shows the mass fraction of chain alkenes (C_8H_{16}) at the center-plane of the cooling channel. In the case of the primary cracking, the mass fraction increases monotonically along the flow direction. In the secondary cracking case, on the other hand, the mass fraction increases initially and then decreases gradually. This is because the fuel undergoes re-cracking as the conversion rate increases. A similar trend is observed for chain alkanes (C_8H_{18}) as well.

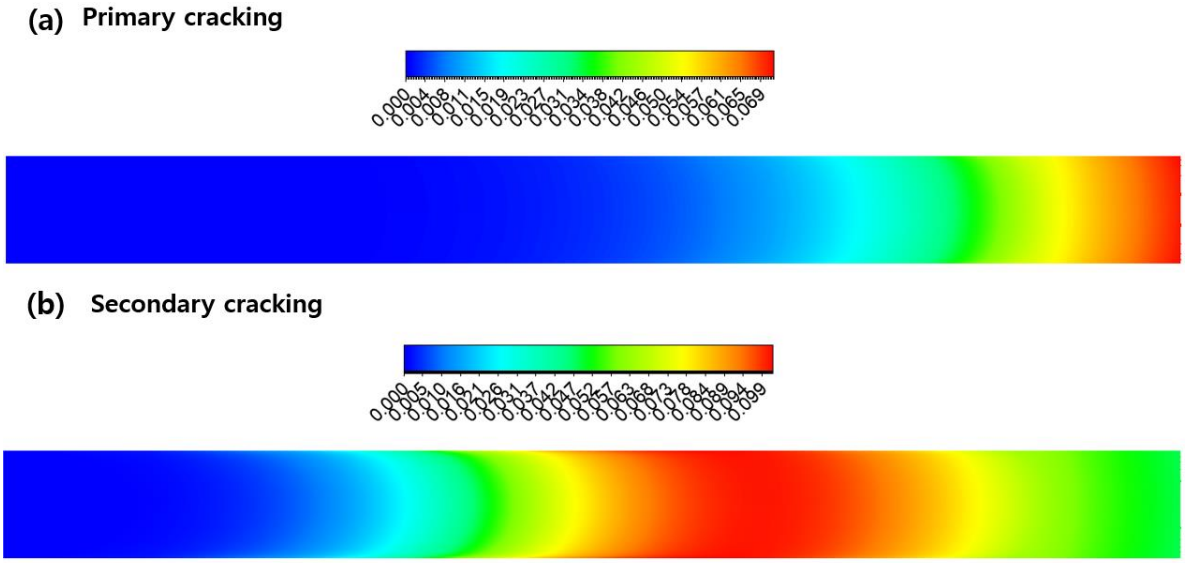

Fig 9. Mass fraction of C_8H_{16} contour in channel fluid domain; (a) Primary cracking, and (b) Secondary cracking

Furthermore, the most apparent characteristics of the secondary cracking is the formation of monocyclic aromatic hydrocarbons (MAH) and cycloalkenes. Fig. 10 illustrates the mass fraction of these chemical species. Both MAH and cycloalkenes show a linear increase with increasing conversion rate, indicating their generation as a result of secondary cracking. This trend is consistent with the experimental data [20].

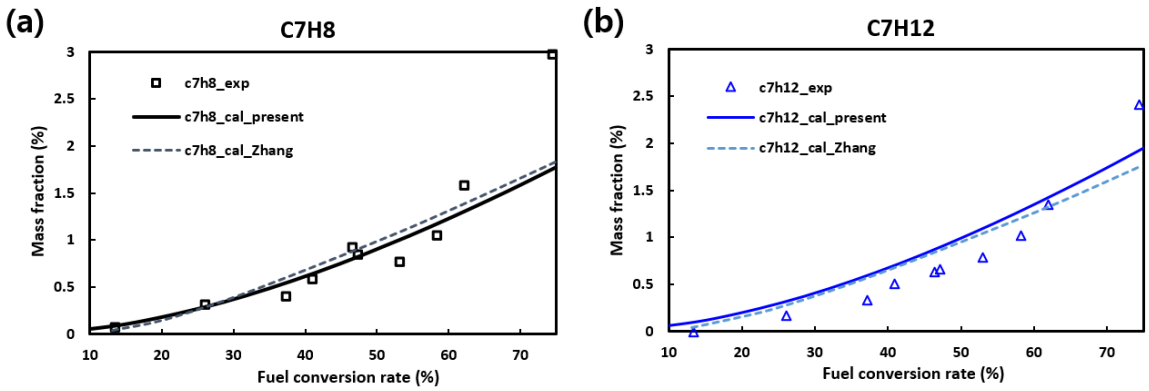

Fig 10. Mass fraction of products species from experiments and numerical simulation; (a) C_7H_8 and (b) C_7H_{12}

Finally, a comparison was made for the major gas and liquid products generated at the conversion rate of 80%. As shown in Figure 11, the mass fractions of the gas species are captured well by the simulation model and closely match the experimental data. Therefore, this study confirms that the numerical analysis of the endothermic decomposition reaction of n-dodecane inside the mini-channel simulates the secondary cracking region quite accurately.

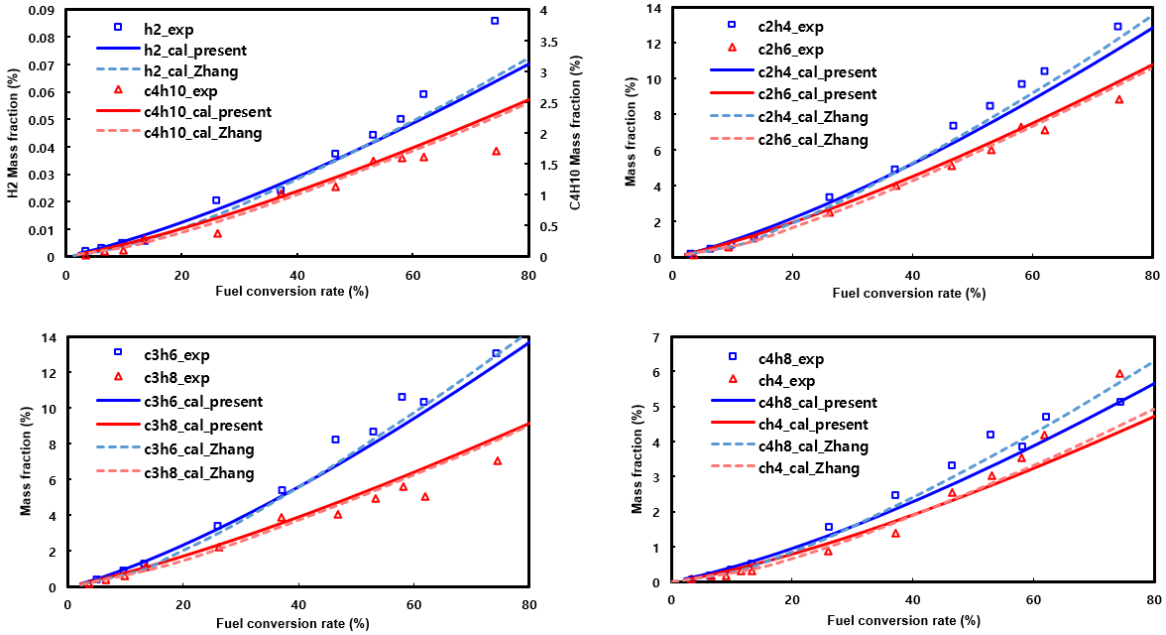

Fig 11. The mass fraction of the product species from experiments and numerical simulations for the secondary cracking

4. Summary and Conclusion

In order to develop an efficient active regenerative cooling system, it is crucial to understand the complex phenomena arising from the pyrolysis reactions in the mini-channels under supercritical conditions. In this study, therefore, a numerical simulation was conducted with the aim of developing an analysis technique for fluid flow, heat transfer, and endothermic decomposition reactions within a single channel.

From the numerical results of flow resistance and heat transfer characteristics, it has been observed that the pressure drop increases and the Heat Transfer Deterioration (HTD) occurs above the pseudo-critical temperature due to the abrupt variation of thermophysical properties near the critical point.

In the simulation of the thermochemical decomposition reaction, the analysis was conducted by dividing it into the primary cracking up to the conversion rate of 13% and the secondary cracking up to the conversion rate of 80%. The analysis applying the Proportional Product Distribution (PPD) model of n-dodecane for primary cracking showed that the increase in the conversion rate and the trend of decreasing temperature due to endothermic decomposition reactions were simulated very nicely. The mass fractions of the generated chemical species increased linearly with increasing conversion rate of n-dodecane, matching the experimental values quite well.

In the simulation including the secondary cracking, a notable feature is the re-decomposition of chain alkanes and chain alkenes, leading to the formation of monocyclic aromatic hydrocarbons (MAH) and cycloalkenes. The analysis results revealed that the mass fraction of chain alkenes (C_8H_{16}) initially increases along the channel length before decreasing due to the re-decomposition. Additionally, it was observed that the mass fractions of MAH, cycloalkenes, and other gas products increase linearly with increasing conversion rate, showing good agreement with the experimental data. Therefore, it is concluded that the simulation effectively captures the thermochemical decomposition reactions occurring inside the mini-channel under supercritical conditions of n-dodecane.

Acknowledgements

This research was supported by Basic Science Research Program through the National Research Foundation (NRF) of Korea funded by the Ministry of Education (2021R1I1A2056769).

References

1. Sziroczak, D., Smith, H.: A review of design issues specific to hypersonic flight vehicles. Prog. Aerosp. Sci. 84, 1-28 (2016)
2. Van Wie, D.M., D'Alessio, S.M., White, M.E.: Hypersonic Airbreathing Propulsion. Johns Hopkins APL Tech. Dig. 4, 430-437 (2005)
3. Glass, D.E.: Ceramic Matrix Composite (CMC) Thermal Protection Systems (TPS) and Hot Structures for Hypersonic Vehicles. In Proceedings of the AIAA International Space Planes and Hypersonic Systems and Technologies Conference, Dayton, OH, USA (2008)
4. Tang, M., Chase, R.L.: The quest for hypersonic flight with air-breathing propulsion. 15th AIAA International Space Planes and Hypersonic Systems and Technologies Conference, Dayton, OH, USA, AIAA, 2008-2546 (2008)
5. Pike, J.: The Choice of Propellants: A Similarity Analysis of Scramjet Second Stages. Philos Trans A. Math. Phys. Eng Sci. 357, 1759 (1999)
6. Edwards, T.: Liquid fuels and propellants for aerospace propulsion: 1903-2003. J. Propuls. Power. (2003). https://doi.org/10.2514/2.6946
7. Cooper, M., Shepherd, J.E.: Experiments studying thermal cracking, catalytic cracking, and pre-mixed partial oxidation of JP-10. 39th AIAA/ASME/SAE/ ASEE Joint Propulsion Conference and Exhibit. Huntsville. AL. USA. AIAA 2003-4687 (2003)
8. Rao, P.N., Kunzru, D.: Thermal cracking of JP-10: Kinetics and product distribution. J. Anal. Appl. Pyrolysis. 76, 154-160 (2006)
9. Kim, J., Hyeon, D.H., Park, S.H., Chun, B.H., Jeong, B.H., Han, J.S., Kim, S.H.: Catalytic endothermic reactions of exo- tetrahydrodicyclopentadiene with zeolites and improvement of heat of reactions. Catal. Today. 232, 63-68 (2014)
10. Sobel, D.R., Spadaccini, L.J.: Hydrocarbon fuel cooling technologies for advanced propulsion. J. Eng. Gas Turbines Power. (1997). https://doi.org/10.1115/1.2815581
11. Boudreau, A.H.: Hypersonic air-breathing propulsion efforts in the Air Force Research Laboratory. 13th AIAA/CIRA International Space Planes and Hypersonic Systems and Technologies Conference. Capua. Italy. AIAA. 2005-3255 (2005)
12. Choi, H., Lee, H.J. Hwang, K.: Research activities about characteristics of fuel injection and combustion using endothermic fuel. KSPE. 17, 4, 73-80, (2013)
13. Zhong, Z., Wang, Z., Sun, M.: Effects of fuel cracking on combustion characteristics of a supersonic model combustor. Acta Astronautica. 110, 1-8 (2015)
14. Li, W., Huang, D., Xu, G., Tao, Z., Wu, Z. and Zhu, H.: Heat transfer to aviation kerosene flowing upward in smooth tubes at supercritical pressures. Int. J. Heat Mass Transf. 85, 1084-1094 (2015)
15. Huang, D., Wu, Z., Sunden, B., Li, W.: A brief review on convection heat transfer of fluids at supercritical pressures in tubes and the recent progress. Appl. Energy. 162, 494-505 (2016)
16. Kim, S.K., Choi, H.S., Kim, Y.: Thermodynamic modeling based on a generalized cubic equation of state for kerosene/LOx rocket combustion. Combust. Flame. 159, 1351-1365 (2012)
17. Zhu, J., Tao, Z., Deng, H., Wang, K., & Yu, X.: Numerical investigation of heat transfer characteristics and flow resistance of kerosene RP-3 under supercritical pressure. Int. J. Heat Mass Transf. 91, 330-341 (2015)
18. Zhang, C.B, Xu, G.Q., Gao, L., Tao, Z., Deng, H.W., Zhu, K.: Experimental investigation on heat transfer of a specific fuel (RP-3) flows through downward tubes at supercritical pressure. J. Supercritical Fluids. 72, 90–99 (2012)

19. Lee, S.H., Wang, Y., Sohn, C.H.: A Numerical Study on the Thermal Decomposition of n-dodecane at Various Mass Flow Rate for Super-critical Condition in a Cylindrical Tube. J. Korean Soc. Combust. 26, 13-19 (2021)
20. Zhang, D., Hou, L., Gao, M., Zhang, X.: Experiment and Modeling on Thermal Cracking of n-Dodecane at Supercritical Pressure. Energy and Fuels. 32, 12426-12434 (2018)